

CALCULATION OF A FREELY-EXPANDING JET OF ARGON INTO A VACUUM PROCESS CHAMBER USING THE DIRECT SIMULATION MONTE CARLO (DSMC) METHOD

Dong Ho Choi – dchoi@usp.br

Universidade de São Paulo, Depto. de Engenharia Mecatrônica e Sistemas Mecânicos
Av. Prof. Mello Moraes, 2231 – São Paulo, SP 05508-900 BRASIL

***Abstract.** The free expansion of Argon injected into a vacuum chamber is simulated using the Direct Simulation Monte-Carlo method. Domains with dimensions up to ten times the hole diameter were simulated with uniform cells of 40 μ m length. The flow is shown to start subsonic, reaching the sonic condition at the exit of the injection hole and continuing to accelerate into the supersonic range. No Mach disks were observed due to the reduced size of the simulation domain. The decay of density along the center line of the injection axis is compared with available experimental data to validate the code. Axisymmetric 2-D distributions of density, temperature, pressure, Mach number, Knudsen number are plotted for some typical conditions. The pressure and the maximum Mach number scale directly with the mass flow rate. The Knudsen number scales inversely with the mass flow rate. Depending on the mass flow rate, the flow regime can traverse the whole range from continuum to free molecular. A discussion is made of the applicability of the continuum and equilibrium hypotheses in the simulation of rarefied gas flows in vacuum chambers.*

***Keywords:** Rarefied, Gasdynamics, Supersonic, Expansion, Simulation*

1. INTRODUCTION

Underexpanded sonic jets have been extensively studied in the past by researchers in the rocket development field. Crist et. al. (1966) and Ashkenas and Sherman (1966) reported experimental observations of Mach disk formation at high pressure ratios in low-density wind tunnels. Bird (1995) has suggested that rarefied gaseous flows may play an important role in modern vacuum processing of semiconductors, which are widely used in the microelectronics industry. A mixture of gases is injected into the vacuum process

chambers that deposit (Chemical Vapor Deposition process) materials onto the Silicon substrate or remove (Reactive Ion Etching process) them, as shown in Fig. 1. The injection of the gas takes place neither symmetrically (i.e., with the injecting hole axis lying on the axis of the chamber) nor perpendicularly to the plane of the top anode. In such a general configuration, a 3-D description of the flow is usually required. However, it is advantageous to simplify the geometry or the domain of study in order to reduce the level of complexity in analysis and simulation. That is accomplished by focusing the study onto the near field of the injector holes, i.e., to the vicinity of the holes, encompassing a length of up to 10 times the diameter of the holes in any direction. Within that volume, the effects of chamber and pumping asymmetries can be neglected and the treatment reduced to that of an axisymmetric geometry. The vicinity of each injection hole can be simplified as shown in Fig. 2. We simplify further by assuming that the holes do not interact with each other, i.e., they are spaced far away from each other.

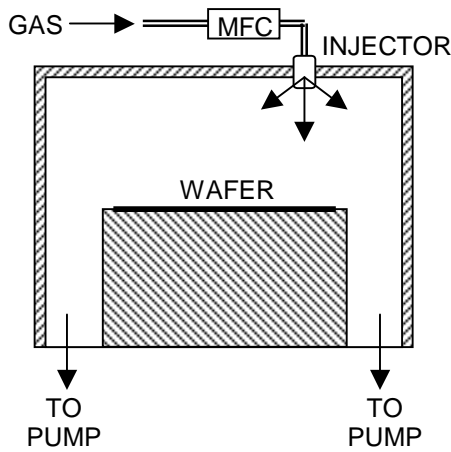


Figure 1 – Schematic of the vacuum chamber: gas goes through the mass flow controller (MFC) and the injector, and expands and travels across the chamber.

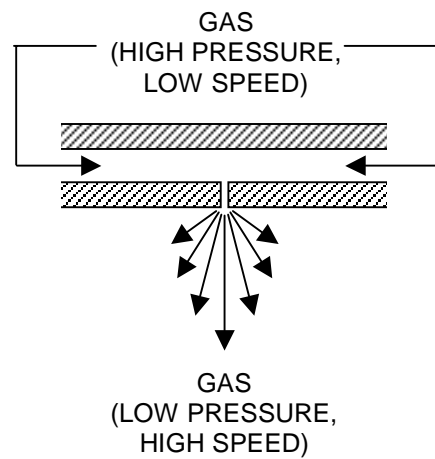


Figure 2 – Schematic of the injector hole.

Table 1: Characteristics of gas injection.

| Parameter | Value |
|----------------------------|----------------------------|
| Number of injection holes | 100 |
| Diameter of each hole | 0.0005 m |
| Length of each hole | 0.002 m |
| Angle (relative to normal) | 80° |
| Mass flow rate | 2.05×10^{-5} kg/s |
| Upstream temperature | 300 K |
| Upstream pressure | > 200 Pa |
| Chamber pressure | 1 – 5 Pa |

Typical characteristics of the injection are shown in Table 1. The gas injected is Argon. Argon is a monoatomic gas, which is relatively simple to simulate since it does not possess rotational nor vibrational energy levels.

The chamber pressure, p_b , is kept low by vacuum pumps. The pressure upstream of the hole, p_{in} , is controlled by the MFC as it tries to supply the desired mass flow. The upstream pressure is close to the stagnation pressure since the flow velocity is low. The gas expands as it travels through the hole, accelerating until it reaches the sonic condition (flow velocity equal to the local sound of speed) somewhere near the exit plane. After it exits the hole, the gas continues to expand into the chamber volume, fanning out radially as well.

Under typical conditions, the gas quickly expands to fill the volume of the chamber. The geometry of the gas injection is seen to exert an influence on the spatial uniformity of the process. It is highly desirable to gain knowledge about the expansion patterns of the gas and its effects on process uniformity. The first step towards that goal is to understand the free expansion of gaseous jets in the vicinity of the exit holes.

2. SIMULATIONS

The basic simulation domain, shown as D_I in Fig. 3, is axisymmetric, with the injector hole of circular cross-section. Molecules of Argon are injected from left to right. The downstream boundaries are vacuum, where the particles that cross that boundary do not return back to the simulation domain. The axis boundary condition was used at $R = 0$ (AXIS) and diffuse reflection boundary condition used at the walls. The domain D_I was divided into 60×60 cells. The hole radius ($= 0.00025\text{m}$) was 6 cells across. Table 2 summarizes the configurations simulated.

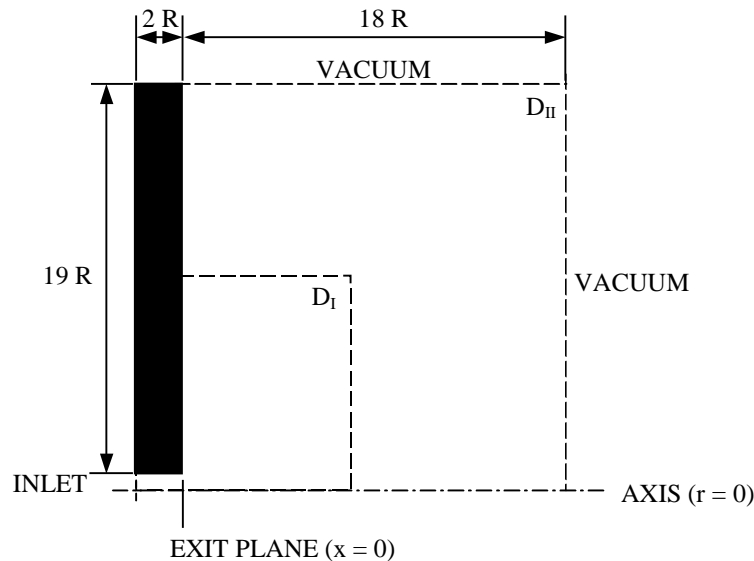


Figure 3 – Simulation domains D_I and D_{II} , with boundary types used.

The DSMC procedure used in this study allowed a reduction in the number of simulated molecules through the parameter M_{real}/M_{sim} . Each simulated molecule represents a large number of real molecules. In our runs, the parameter M_{real}/M_{sim} was varied to keep the number of simulated molecules on the order of 10^4 . The reduced number of molecules gives rise to unacceptably large statistical scatter of instantaneously sampled variables.

Time averaging is done for steady flows to increase the number of samples and thus reduce the scatter.

Table 2. Summary of all cases simulated.

| Run # | $M_{\text{real}}/M_{\text{sim}}$ | $\Delta t_{\text{motion}} \times 10^6$ (s) | $n_{\text{jet}} \times 10^{-22}$ (m ⁻³) | V_{jet} (m/s) | T_{jet} (K) | $\dot{m} \times 10^5$ (kg/s) | Mach | Domain |
|-------|----------------------------------|--|---|------------------------|----------------------|------------------------------|------|-----------------|
| 1 | 1×10^6 | 1.0 | 0.01 | 322.4 | 300 | 0.00451 | 1.00 | D _I |
| 2 | 4×10^8 | 0.1 | 4.55 | 322.4 | 300 | 2.06 | 1.00 | D _I |
| 3 | 5×10^9 | 0.1 | 105 | 322.4 | 300 | 47.5 | 1.00 | D _I |
| 4 | 1×10^{11} | 0.004 | 2000 | 322.4 | 300 | 1131 | 1.00 | D _I |
| 5 | 1×10^6 | 5.0 | 0.01 | 693.4 | 300 | 0.00973 | 2.15 | D _I |
| 6 | 3×10^8 | 0.1 | 3.26 | 450.0 | 300 | 2.06 | 1.40 | D _I |
| 7 | 2×10^8 | 0.1 | 2.44 | 600.0 | 300 | 2.05 | 1.86 | D _I |
| 8 | 4×10^9 | 0.1 | 56.5 | 600.0 | 300 | 47.6 | 1.86 | D _I |
| 9 | 8×10^9 | 0.1 | 169 | 200.0 | 300 | 47.4 | 0.62 | D _I |
| 10 | 4×10^8 | 0.1 | 4.55 | 322.4 | 300 | 2.06 | 1.00 | D _{II} |

Observation: the mass flow figures were calculated assuming 4×27 holes of diameter 0.0005m.

The parameter Δt_{motion} sets the time step over which we artificially decouple molecular motions from collisions, i.e., we follow the motion of molecules using the time step Δt_{motion} and sample for collisions every fixed number of Δt_{motion} intervals. Thus, we have the relationship:

$$\Delta t_{\text{motion}} \ll \frac{1}{\nu_{\text{coll}}} \quad (1)$$

where ν_{coll} is the collision frequency. In general, the simulation yields more exact results with smaller time steps and cell sizes. The DSMC procedure also defined sub-cells within each cell, that allowed better representation of collisions and produced more realistic vortical flows.

Steady-state is reached within a relatively small number of Δt_{motion} steps (typically on the order of 100 to 1000 steps). The remainder of the run was spent accumulating samples to overcome the statistical scatter caused by the smaller number of molecules being simulated. Typical runs encompassed 10000 Δt_{motion} steps, which are sufficient to reduce the scatter of the instantaneous dependent variables.

Most runs were made imposing an inlet flow in the form of a jet at sonic condition. The mass flow rate, \dot{m} (in kg/s), is a function of the number density, n_{jet} (in molecules/m³), and the temperature, T_{jet} (in Kelvin), according to the expression:

$$\dot{m} = 6.62 \times 10^{-26} n_{\text{jet}} \sqrt{\gamma R T_{\text{jet}}} A^* \quad (2)$$

where γ is the ratio of specific heats (= 5/3 for Argon), R is the gas constant (= 207.85 J/K for Argon) and A^* is the area of the injection hole (= 1.96×10^{-7} m²). For $T_{\text{jet}} = 300$ K, n_{jet} becomes a function solely of \dot{m} .

The domain for run #10, D_{II} , was increased by a factor of 2 over D_I , consisting of 120×120 cells. This was done to check for the effect of the downstream boundaries. The two domains are shown in Figure 3.

The longest of the runs in Table 2 took approximately 3 days using a Pentium II class personal computer, with 64MB of RAM, running at 200MHz in a Windows NT environment.

3. RESULTS

Each simulation outputs the density, ρ , temperature, T , and velocity components, (V_x, V_r, V_θ) , in each of the cells of the domain. With them, the pressure, p , Mach number, M , and local Knudsen number, Kn , are calculated following the expressions below:

$$p = nkT, \quad k = 1.38 \times 10^{-23} \text{ J/K (Boltzman's constant)} \quad (3)$$

$$M = \frac{\sqrt{V_x^2 + V_r^2}}{\sqrt{\gamma R T}}, \quad \text{where } V_\theta \approx 0 \quad (4)$$

$$Kn = \frac{\lambda}{\ell} = \frac{1}{\sqrt{2\pi} d^2 n} = \frac{1}{\sqrt{2\pi} d^2 n} \frac{\sqrt{\left(\frac{d\rho}{dx}\right)^2 + \left(\frac{d\rho}{dr}\right)^2}}{\rho} \quad (5)$$

The density n in the equations above is the number density, given in molecules/ m^3 . The local Knudsen number is the ratio between the mean free path, λ , and a characteristic length, ℓ , estimated using both components of the density gradient vector. We used the molecular diameter $d = 4.17 \times 10^{-10} m$ for Argon. The flow is considered to be in the continuum regime for $Kn < 0.1$ and in the free molecular regime for $Kn > 1$.

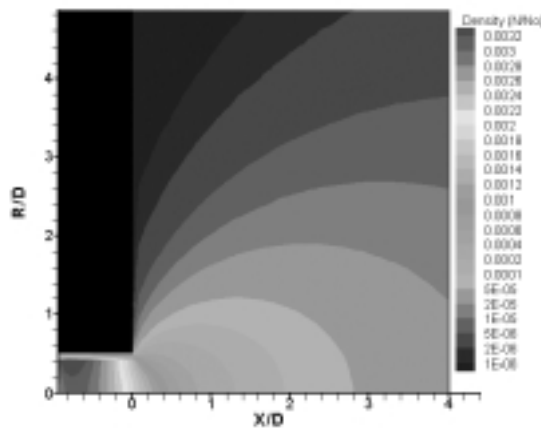


Figure 4 – Density distribution (n/n_0) for Run #2.

Figure 4 shows the 2-D plot of density for Run #2. The spatial coordinates were normalized with respect to the hole diameter and the density with the density n_0 at standard

conditions of pressure and temperature ($= 2.69 \times 10^{25}$ molecules/m³, at 300K and 1atm). The centerline values of density, temperature, pressure, Mach number and Knudsen number, are shown in Figure 5. The density increases a little at the entrance of the hole and falls off rapidly as the gas accelerates through the remainder and out of the hole. The temperature and pressure decrease in the same trajectory, while the Mach number begins at around 0.5, reaches 1.0 at the exit plane and keeps on increasing until it settles to ≈ 5 for $X/D \approx 2$. The Knudsen number is less than 0.1 inside the hole but quickly increases away from the exit plane ($X/D < 0.2$). Most of the flow in the domain occurs with $Kn > 0.1$, i.e., away from the continuum regime.

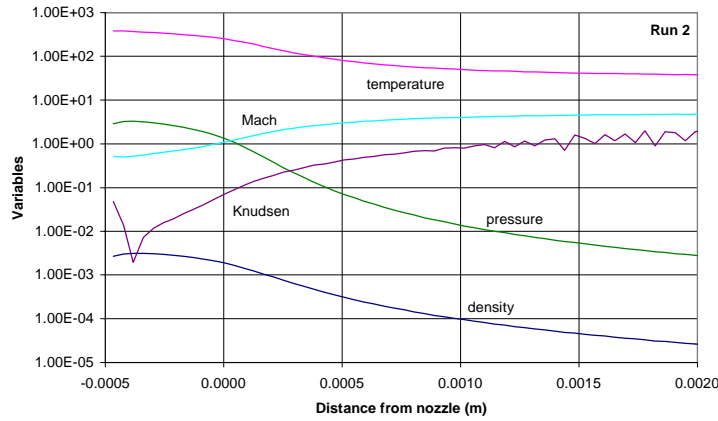


Figure 5 – Plots of flow properties on the centerline. Run #2.

The centerline density data was normalized with respect to the value at the exit plane and plotted in Figure 6, together with the experimental data by Mombo-Caristan et al. (1988). The agreement between the predicted curve and the measured values is remarkable, considering that the simulation data corresponds to a pressure ratio of $p_{in}/p_b = 1230$ (with $p_{in} = 420$ Pa) while the experimental data correspond to a pressure ratio of $p_{in}/p_b = 750$ (with $p_{in} = 1.5 \times 10^5$ Pa).

Ashkenas and Sherman (1966) stated that, for transition flows, the Mach disk increases in thickness until it disappears altogether when the flow becomes very rarefied (free molecular regime). The theoretical position of the Mach disk derived by their data is:

$$\frac{X_M}{D} = 0.67 \sqrt{\frac{p_{in}}{p_b}} \approx 0.67 \sqrt{\frac{3.2}{0.0026}} = 23.5 \quad (6)$$

The numerical values are from Run #2. The Mach disk, or what would be left of it in the rarefied regime, is estimated to be located well outside of the simulation domain.

Figures 7 through 10 show the distributions of temperature, pressure, Mach number and Knudsen number for Run #2. The initial jet spreads radially to fill the whole domain, without allowing any vortices to be formed. They show the localization of the jet in the immediate vicinity of the injection hole. The distribution of pressure is very similar to that of density, as can be seen from Figures 4, 5 and 8.

Runs 1 through 9 give qualitatively similar 2-D plots of the properties considered. Therefore, we will not plot them individually here. We will present, instead, the results of

some comparisons we have made of the pressure ratios and the Mach and Knudsen numbers among the various configurations simulated.

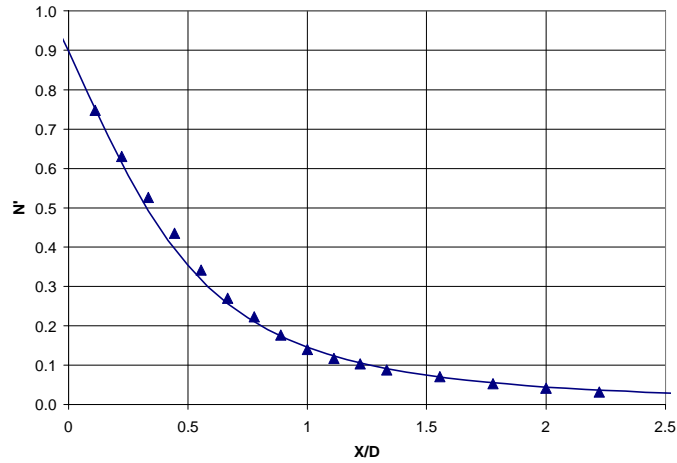


Figure 6 – Centerline normalized densities: line = simulated data (Run #2); symbol = experimental data by Mombo-Caristan.

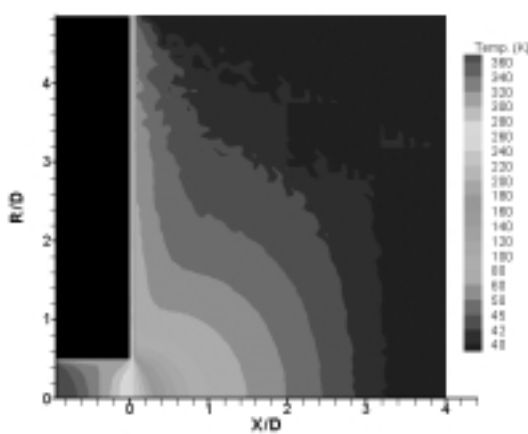


Figure 7 – Temperature distribution for Run #2.

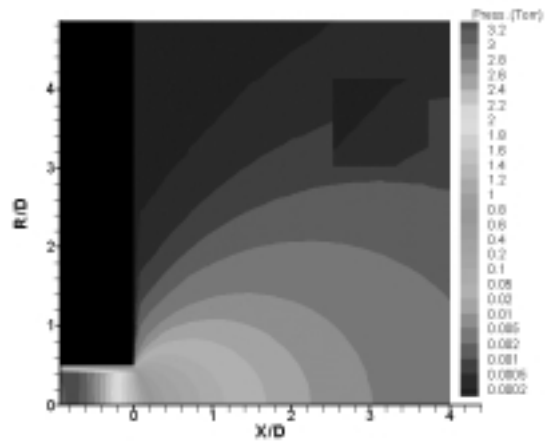


Figure 8 – Pressure distribution for Run #2.

Table 3 summarizes some relevant centerline parameters for all runs. The subscript 'jet' refers to the input properties in the DSMC procedure, the subscript 'in' to the hole inlet, the subscript 'b' to the far side (outermost X-boundary), the subscript 'exit' to the plane of X=0.

Runs 2, 6 and 7 correspond to a mass flow rate of 1.9×10^{-7} kg/s. The jet velocities, and accordingly the densities, were varied keeping the temperature fixed at 300K. The program reached equilibrium keeping the exit Mach number at unity and varying the jet temperature to pass the required flow. The following observations can be made:

- i) p_{in} , p_b , (p_{in}/p_b) and $(n/n_o)_{exit}$ scale directly with n_{jet} , while M_{in} , M_b , Kn_b and T_{exit} scale inversely with n_{jet} .
- ii) All inlet Mach numbers correspond to subsonic conditions. Supersonic inlet conditions do not happen unless they are designed into the system. The program tries to satisfy the

total mass flow rate by varying the inlet pressure at a given temperature. If the temperature increases, the inlet pressure required will decrease.

- iii) For a total flow of 1.9×10^{-7} kg/s, the Knudsen numbers at the far side are on the order of 2, which places the flow in the free molecular regime. If multiple injection holes are used, the total density in the chamber will increase proportionally to the number of injection holes. The Knudsen number, which is inversely proportional to density, will decrease proportionally. If 20 or more holes are used, the Knudsen number will be less than 0.1 – a value that places the flow in the continuum regime when a Mach disk can appear.
- iv) The pressure ratio p_{in}/p_b is much larger than the value needed to reach sonic conditions (≈ 2). The bulk of the pressure drop occurs in the free expansion during which the flow becomes supersonic.

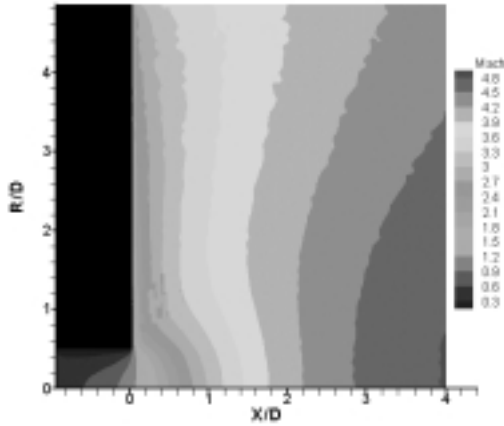


Figure 9 – Mach number distribution for Run #2.

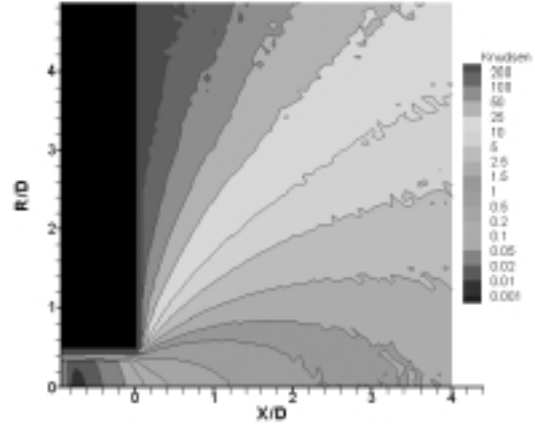


Figure 10 – Knudsen number distribution for Run #2.

Table 3. Summary of centerline parameters.

| Run | $n_{jet} \times 10^{-22}$ (m^{-3}) | p_{in} (Pa) | p_b (Pa) | p_{in}/p_b | Kn_b | M_{in} | M_b | $(n/n_o)_{exit}$ $\times 10^3$ | T_{exit} (K) |
|-----|---|------------------|---------------|--------------|--------|----------|-------|-----------------------------------|-------------------|
| 1 | 0.01 | 0.93 | 0.0016 | 574 | 519 | 0.371 | 3.51 | 0.0040 | 272 |
| 2 | 4.55 | 380 | 0.353 | 1076 | 2.12 | 0.515 | 4.80 | 2.12 | 272 |
| 3 | 105 | 8490 | 4.32 | 1968 | 0.088 | 0.548 | 7.71 | 47.3 | 284 |
| 4 | 2000 | 167800 | 90.9 | 1845 | 0.0096 | 0.542 | 7.39 | 892 | 297 |
| 5 | 0.01 | 1.50 | 0.0059 | 249 | 327 | 0.565 | 4.29 | 0.0060 | 395 |
| 6 | 3.26 | 306 | 0.365 | 839 | 2.13 | 0.617 | 4.55 | 1.80 | 303 |
| 7 | 2.44 | 262 | 0.417 | 627 | 2.08 | 0.770 | 4.43 | 1.62 | 353 |
| 8 | 56.5 | 5990 | 4.79 | 1250 | 0.11 | 0.813 | 7.52 | 33.2 | 411 |
| 9 | 169 | 11600 | 5.13 | 2263 | 0.057 | 0.475 | 7.75 | 66.7 | 245 |
| 10 | 4.55 | 380 | 0.349 | 1089 | 1.96 | 0.513 | 4.83 | 2.12 | 272 |

Runs 3, 8 and 9 correspond to a mass flow rate of 4.3×10^{-6} kg/s. The same trends are observed as in the previous section. Comparing the orders of magnitude of the properties in the two tables, we can make following observations:

- v) The values of the Knudsen number are lower, ensuring that the flow from multiple nozzles will result in the flow being closer to the continuum regime.
- vi) P_{in} and p_{in}/p_b are much larger than the values for 1.9×10^{-7} kg/s. The larger values of p_{in} (at roughly the same enthalpy) are required to pass the bigger flow rate. The larger values of the pressure ratio mean that the driving force for the free expansion increases with increasing flow rate, which is evidenced by the larger values of far-side Mach numbers (7.5 as opposed to 4.5). Notice that the inlet Mach numbers are still subsonic and not much different from the previous case.

Table 4 summarizes the correlation between \dot{m} , n_{in} , p_{in} and $(n/n_o)_{exit}$ for simulations where the jet was specified to be sonic at a temperature of 300K. n_{in} , p_{in} and $(n/n_o)_{exit}$ scale directly with \dot{m} . Furthermore, $(n/n_o)_{exit}$ is linearly proportional to p_{in} , reproducing one of the fundamental results of the theory of compressible flows - that the mass flow rate of a choked nozzle varies linearly with the stagnation pressure. We obtained:

$$\left(\frac{n}{n_o} \right)_{exit} = 9.2 \times 10^{-2} p_{in} \quad (7)$$

Run #10 was a repetition of run #2, with the domain doubled, as schematized in Figure 5. It showed that very little changed with the increased domain, which allow us to conclude that the outgoing boundary effects are negligible. This may be the case because of the vacuum boundary conditions we used throughout these runs.

Table 4. Summary of correlations for M=1 runs.

| Run | \dot{m} (kg/s) | $n_{jet} \times 10^{-22}$ (m^{-3}) | p_{in} (Pa) | $(n/n_o)_{exit}$ |
|-----|-----------------------|---|--------------------|-----------------------|
| 1 | 4.2×10^{-10} | 0.01 | 0.93 | 4.05×10^{-6} |
| 2 | 1.9×10^{-7} | 4.55 | 380 | 2.12×10^{-3} |
| 3 | 4.4×10^{-6} | 105.00 | 8490 | 4.73×10^{-2} |
| 4 | 1.05×10^{-4} | 2000.00 | 1.68×10^5 | 8.92×10^{-1} |

4. CONCLUSION

The numerical simulation of a jet of Argon expanding through a finite size nozzle and expanding into a vacuum chamber was done using the Direct Simulation Monte Carlo method. The axisymmetric injection geometry was divided into cells and the movement of a reduced number of simulated molecules was calculated together with accompanying collisions between molecules and between molecules and the walls. The computing requirements were satisfied by personal computers and execution times were of the order of a day.

The flow was shown to start subsonic, reaching the sonic condition at the exit of the injection hole and continuing to accelerate into the supersonic range. No Mach disks were observed due to the reduced size of the simulation domain. The decay of density along the center line of the injection axis was compared with available experimental data to validate the code. Axisymmetric 2-D distributions of density, temperature, pressure, Mach number, Knudsen number for some typical conditions showed that the flow in the regions close to

the exit plane and wide angles (with respect to the axis) was not in the continuum regime. Bird (1995) argues that the attainment of equilibrium conditions roughly scale with that of the continuum regime. Where the continuum hypothesis breaks down, equilibrium is likely not to hold as well. The pressure and the maximum Mach number scaled directly with the mass flow rate. The Knudsen number scaled inversely with the mass flow rate. Depending on the mass flow rate, the flow regime could traverse the whole range from continuum to free molecular.

The ratio between the inlet pressure and the chamber pressure resulted much larger than 2, which is the pressure ratio required for isentropic choking (attaining the sonic condition at the exit of the nozzle) of Argon. The large pressure gradient between the nozzle exit and the chamber drives the free expansion process through which the jet opens up radially as it travels away from the exit.

On the practical side, it was suggested that the total mass flow rate be distributed across as many holes as possible, to reduce the pressures and Mach numbers and increase the distance of a likely Mach disk from the wafer process area. However, it has the deleterious effect, through the increase of the Knudsen number with decreasing mass flow rate, of allowing background gases to penetrate more easily into the jet and deposit on the wall close to the nozzle exits.

No vortical flows were observed in the simulations, because the Knudsen numbers were generally high. It is expected that, as multiple nozzles are used and the density and pressure in the chamber increases, vortical flow patterns will appear, which will aid in the transport of polymer precursor radicals from the plasma bulk region onto the walls adjacent to the injection nozzles. This is an area of investigation that, together with simulations with finite pressure boundaries and flows of more complex gases, deserves more attention in the future.

Acknowledgements

The author would like to acknowledge the financial support of Applied Materials Inc.

REFERENCES

- Ashkenas, H. & Sherman, F. S., 1966, The structure and utilization of supersonic free jets in low density wind tunnels, *Rarefied Gas Dynamics, Fourth International Symposium, Supplement 3, vol. 2*, ed. by J. H. de Leeuw, Academic Press, New York, p. 84.
- Bird, G. A., 1995, *Molecular Gas Dynamics and the Direct Simulation of Gas Flows*, Clarendon, Oxford.
- Crist, S., Sherman, P. M., & Glass, D. R., 1966, Study of the highly underexpanded sonic jet, *AIAA Journal*, vol. 4, number 1, pp. 68–71.
- Mombo-Caristan, J. C., Philippe, L. C., Chidiac, C., Perrin, M. Y. & Martins, J. P., 1989, Measurements of freejet densities by laser beam deviation, *Rarefied Gas Dynamics, Sixteenth International Symposium, vol. 117*, ed. by E. P. Muntz, D. P. Weaver & D. H. Campbell, AIAA, Washington, pp. 140–148.